# Few-Cycle Surface Plasmon Polariton Generation by Rotating Wavefront Pulses

F. Pisani,*,[†] L. Fedeli,*,[‡] and A. Macchi*,[¶],[†]

[†]Enrico Fermi Department of Physics, University of Pisa, 56127 Pisa, Italy

[‡]Department of Energy, Politecnico di Milano, 20133 Milano, Italy

[¶]National Institute of Optics, National Research Council (CNR/INO), A.Gozzini unit, 56124 Pisa, Italy

Ⓢ Supporting Information

ABSTRACT: A concept for the efficient generation of surface plasmon polaritons (SPPs) with ultrashort duration close to the single-cycle limit is presented. The scheme is based on grating coupling and laser pulses with wavefront rotation (WFR), so that the resonance condition for SPP excitation is satisfied only for a time window shorter than the driving pulse. The feasibility and robustness of the technique is investigated by means of simulations with realistic parameters. In optimal conditions, we find that a 29.5 fs pulse with an 800 nm wavelength can excite SPPs with <4 fs duration (∼1.5 laser cycles) and a peak field amplitude ∼2.7 times the peak value for the laser pulse.

KEYWORDS: ultrashort pulses, femtosecond plasmonics, grating-coupler, few-cycle plasmonics, strong coupling
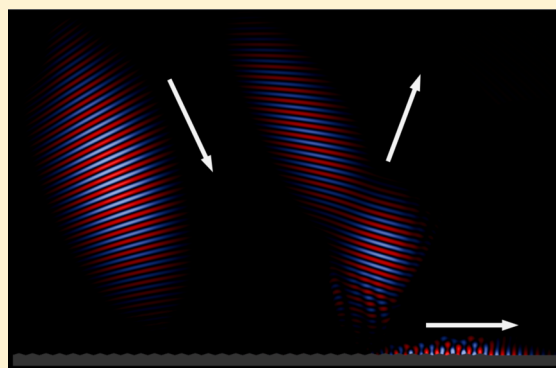
Ultrafast plasmonics raised great interest in the last decades. Surface plasmons (SPs) with ultrashort, i.e., few-cycle, duration may yield high temporal resolution in plasmonic-based techniques, which have found widespread diffusion in the material science community, such as molecular sensing[1] or surface-plasmon-enhanced spectroscopy (SERS).[2−5] Ultrafast plasmonic switches and modulators[6,7] also suggest possible applications in the next generation of photonic circuits.[8−10] The generation of SPs with a duration close to the single-cycle limit is attractive in general because it would add the extreme compression in the temporal domain to the known SP potential to concentrate the light beyond the diffraction limit, so that the electromagnetic (EM) energy would be effectively focused in a "sub-wavelength-cube" volume. This approach is very promising for the study of strong field phenomena at relatively low laser energy,[11] including recently developed approaches to surface plasmon polariton (SPP)-enhanced emissions in the domain of relativistic electron dynamics.[12−14] Close to the single-cycle limit, the phase of the oscillation strongly characterizes the field of the SP, opening the possibility to extend the study of effect of the carrier envelope phase (CEP)[15−19] in the domain of plasmonics.

Of particular interest is the development of ultrafast photocathodes[20,21] to enable electron-based investigations of ultrashort phenomena such as the effects of the vibration of a lattice on the electric and thermal transport[22] and molecular chemical processes.[23] In this context, using the Kretschmann prism configuration to excite propagating SPPs on a metallic

surface, Dombi et al.[11] demonstrated via electron photo-emission and optical acceleration the excitation of SPPs having a duration in the 5.6−9 fs range, slightly longer than the 5 fs duration laser pulse driver and corresponding to 2 or 3 oscillations of the field.

In this paper we present a concept to efficiently generate ultrashort SPPs with a duration of less than two laser cycles, using a driver with a much longer duration of ∼10 cycles. The proposed method is based on laser pulses with wavefront rotation (WFR) impinging on a metallic grating. The use of a grating[24] is a well-known method to couple an EM wave to an SPP, which is also suitable for high-intensity drivers since the latter do not cross layers of material as in the Kreschmann configuration. When the plasma frequency of the grating material is much greater than the laser frequency, the condition for resonant SPP excitation[25] is satisfied for values θ_R of the incidence angle θ, which are solutions of the equation

$$\sin \theta \simeq 1 \pm n \frac{\lambda}{d} \tag{1}$$

where λ is the laser wavelength, d is the grating pitch, and n is an integer number (in the following we restrict it to the $|n| = 1$ case). In a laser pulse with WFR, the resonance condition will be satisfied only for a short time interval since the rotation of the fronts of constant phase is equivalent to a continuous temporal variation of the local angle of incidence. As a

consequence, the generation of an SPP with a duration much shorter than the impinging laser pulse is expected. By coupling the grating target with a suitable nanostructure,[26] the propagating SPPs may also be used to excite localized SPs with few-cycle duration.

WFR can be obtained by focusing a pulse with the wavefronts tilted with respect to the direction of propagation.[27,28] Heuristically, different portions of the laser pulse reach the focus at different times and with different directions of propagation; thus a pulse with wavefronts rotating in time is observed at the focus. The expression of a Gaussian pulse with WFR at focus is (see refs 29 and 30 for a more detailed description)

$$E(r, t) = E_0 \exp\left[-\frac{r^2}{w_0{}^2} - \frac{t^2}{\tau^2}\right] \exp[i\varphi(r, t)] \tag{2}$$

$$\varphi(r, t) = 4\frac{w_i \eta}{w_0 \tau_f \tau_i} rt + \omega_L t \tag{3}$$

where ω_L is the laser frequency, τ_f, w_0, and r are respectively the pulse duration, waist, and transverse coordinate in the focus, τ_i and w_i are the duration and the waist before focusing, and η is the pulse front tilt parameter. Notice that the pulse is characterized by spatiotemporal coupling; that is, in the expression of the EM field the spatial and temporal dependences cannot be separated $[E(\mathbf{r}, t) \neq E_0 S(\mathbf{r}) T(t)]$. The rotation velocity of the phase front is given by

$$v_r = \frac{c}{\omega_L} \frac{\partial^2 \varphi(r, t)}{\partial r \, \partial t} \tag{4}$$

In their experiment, Quéré et al.[27] demonstrated the possibility to control the rotation velocity and obtained a value of $v_r \simeq 14.6$ mrad/fs. A maximum achievable value of ~30 mrad/fs was also estimated with their setup, so that a 30 fs laser pulse would span a ~50° arc.

We performed a two-dimensional (2D) simulation campaign to test the effectiveness and robustness of the proposed concept. As will be shown below, the simulations demonstrate that an SPP shorter than 1.5 laser cycles may be generated, with a peak value of the field nearly 3 times the value for the driving pulse and an energy conversion efficiency of >5%.

■ RESULTS AND DISCUSSION

In the simulations, performed using the MEEP code (see Methods), silver was selected as the grating material, which is a typical choice in plasmonics.[1,31−33] The linear response is described by the dielectric function

$$\varepsilon(\omega) = 1 - \frac{\omega_P{}^2}{\omega^2 - i\gamma\omega} \tag{5}$$

with the plasma frequency ω_P = 9.6 eV (6.8×10^{14} s^{-1}) and the damping coefficient γ = 0.0228 eV (values from ref 34). The wavelength of the laser pulse was λ = 800 nm (Ti:sapphire). While we are restricted to a specific material and laser source for simplicity and brevity, our concept does not depend on this particular choice.

In Figure 1(a) the basic simulation setup is shown. The laser pulse impinges in the middle of the grating coupler, which is ~25 μm wide. On the right side of the target, where the SPP propagates, the surface is flat. The laser focus was at a distance of 15 μm from the target. Figure 1(b) shows a snapshot of a
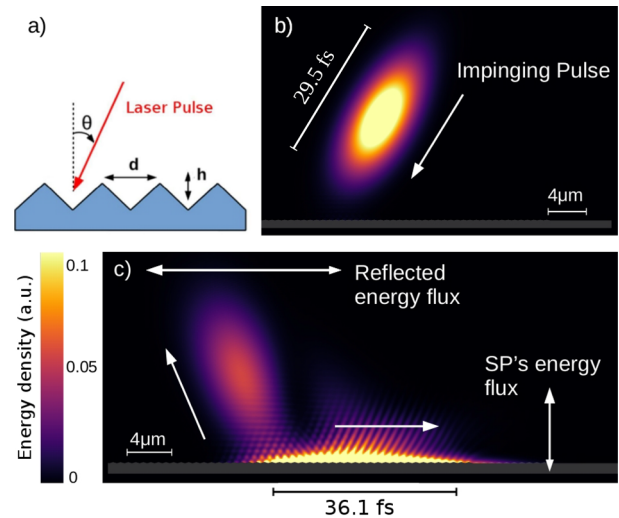

Figure 1. (a) Schematic setup of the simulation box. (b) 2D map of the EM energy density (cycle-averaged) showing a pulse without WFR impinging on the grating (shown in gray). (c) Same as (b) at later times, showing the excited SPP propagating along the grating surface and the reflected pulse. The associated energy fluxes are measured through the marked vertical and horizontal lines.

laser pulse (without WFR) impinging on the grating at the resonant angle. Figure 1(c) shows the excited SPP and the reflected pulse. The energy fluxes of the reflected pulse and SPP are measured through the marked vertical and horizontal lines. Notice that the SPP has a longer duration than the driving laser pulse.

In order to optimize the coupling efficiency, a preliminary study has been performed by varying both the parameters of the laser pulse and of the grating, i.e., the depth and width of the grooves and the profile shape (triangular, rectangular, sinusoidal, and sawtooth-like). The efficiency was maximal for a triangular grating having a depth h = 140 nm and pitch d = 0.56 μm, corresponding to the resonance angle θ_R = −25° (the negative value of the incidence angle corresponds to the SPP propagating in the opposite direction with respect to $k_{\parallel}$, the component of the laser pulse wavevector parallel to the surface). The maximum of the coupled energy (i.e., the percentage of the pulse energy transferred to the material) was 61% of that of the laser pulse. The energy transferred to the SPP, measured after ~30 fs from the generation and after a propagation of ~12 μm along the surface, was 38%. The remaining fraction of the coupled energy was either re-emitted during the propagation along the grating region or absorbed in the material.

Figure 2 shows a snapshot of the field for the same parameters of Figure 1 but using a pulse with WFR. The rotation of the wavefronts has been set in order to have the central wavefront (i.e., the phase front corresponding to the maximum intensity) impinging at an angle $90° − \theta_R$ on the target, so that the instantaneous angle of incidence has the resonant value at the pulse peak. An SPP shorter than the laser pulse is generated near the peak of the pulse. In coincidence to the SPP excitation, a narrow "hole" is produced in the profile of the reflected pulse corresponding to the transient decrease in the reflectivity of the grating.

The laser pulse parameters, including the WFR velocity, were varied in the simulations in order to determine the shortest duration of the SPP. Figure 3(a) shows the energy flux of the
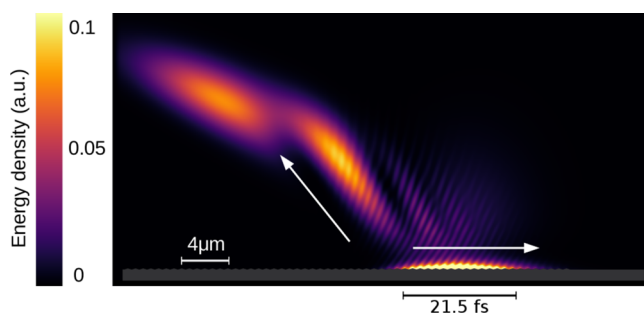
Figure 2. EM energy density after the interaction of a WFR pulse with the grating. An SPP with a duration shorter than the laser pulse is generated. The reflected pulse profile shows a narrow minimum ("hole") corresponding to the SPP excitation near the pulse peak.
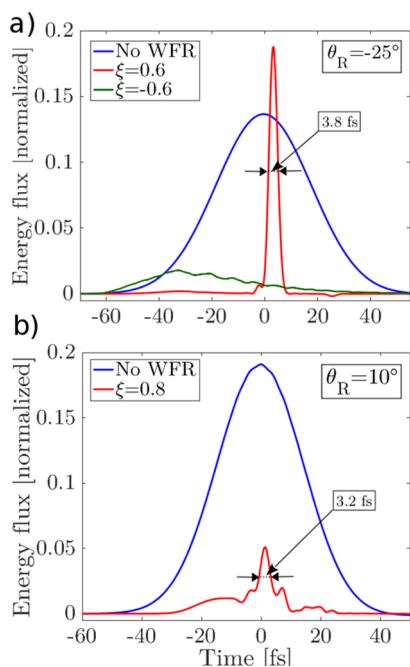

Figure 3. (a) Energy fluxes (normalized to the energy flux of the laser pulse) of SPPs generated on a grating by laser pulses incident at the resonant angle $\theta_R = -25°$ and different WFR velocities $\xi = 0$ (blue curve), $\xi = 0.6$ (red curve), and $\xi = -0.6$ (green curve). The laser pulse duration and waist size are ∼29.5 fs and 4.8 μm, respectively. (b) Same as (a) but for $\theta_R = 10°$ and $\xi = 0$ (blue curve) and $\xi = 0.8$ (red curve).

SPPs generated on the grating with pitch $d = 0.56$ μm ($\theta_R = -25°$) by a WFR pulse with a duration of ∼29.5 fs and a waist size $6\lambda = 4.8$ μm. Using a rotation parameter $\xi = 0.6$, the SPP has a duration of ∼3.8 fs, i.e., 1.4 laser cycles at full-width at half-maximum (fwhm). The energy coupling efficiency is 5.6%, and the peak amplitude of the SPP field is ∼2.7 times the peak amplitude of the laser pulse. The intensity of the ultrashort SPP is also higher (by ∼35%) than the intensity of the SPP generated without WFR.

The intensity increase (which will be further discussed below) shows a clear advantage of the WFR approach with respect to the alternative idea of exploiting the laser bandwidth to produce a longitudinally chirped pulse with the frequency varying along the propagation direction so that the laser frequency is resonant with that of the SPP only for a portion of the pulse. In this case, the driving pulse is stretched in time and has a lower intensity, resulting in a low efficiency and modest
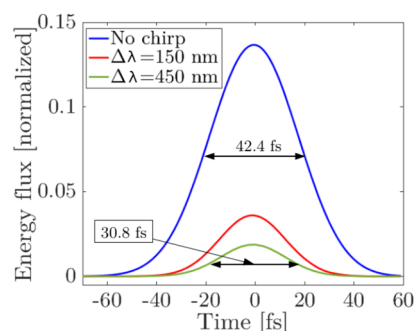
Figure 4. Energy fluxes (normalized to the energy flux of the laser pulse) of SPPs generated on a grating by laser pulses with a chirp $\Delta\lambda$ incident at the resonant angle $\theta_R = -25°$ for the central frequency. The laser pulse duration and waist size are ∼29.5 fs and 4.8 μm, respectively.
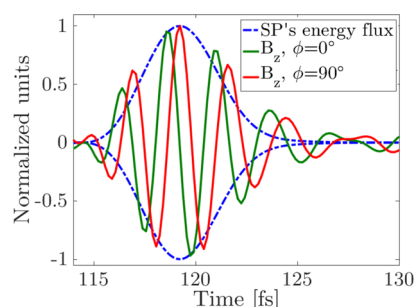

Figure 5. Energy flux (dotted line) and magnetic field (continuous lines) as a function of time for two SPPs of ∼3.8 fs duration generated by two WFR laser pulses with $\xi = 0.6$ and different values of the CEP ϕ (0° and 90°). Other parameters are the same as in Figure 3(a). The SPP generated for $\phi = 90°$ shows a significant asymmetry in the waveform.

shortening effect as we verified via our simulations (Figure 4). It may be worth noticing that the WFR pulse also exploits the laser bandwidth, as it can effectively be considered to have a *transverse* chirp with the frequency varying in the direction perpendicular to the propagation.

The duration of the SPP is short enough for the absolute phase of the field oscillation to be important for the SPP characterization. Figure 5 shows the energy flux and the magnetic field as functions of time for the same ultrashort SPP of Figure 3(a) and an SPP generated in identical conditions but for the value of the CEP ϕ of the laser pulse, which differs by 90°. The two values of ϕ yield an SPP with zero and 11% asymmetry, defined as the relative difference between the absolute values of the maximum and the minimum of the field.

Using extremely high values of ξ is found to affect the envelope of the SPPs. As an example Figure 3(b) shows a case analogous to Figure 3(a) for $\theta_r = 10°$ ($d = 0.98$ μm), in which the effect of $\xi = 0.8$ is compared to $\xi = 0$. The SPP shows significant modulations with a central peak having a duration of ∼3.2 fs (1.2 laser cycles) and energy flux characterized by several secondary peaks with an intensity comparable to that of the main one. Such a modulated SPP might not be suitable for all the foreseen applications of ultrashort plasmonics.

Notice that the direction of the WFR, i.e., the sign of the rotation parameter ξ, is crucial for the ultrashort SPP generation. As also shown in Figure 3(a), the SPP generated with $\xi = -0.6$ has a fwhm duration of 39.6 fs, i.e., longer than that of the driving pulse, and a very low intensity. This effect
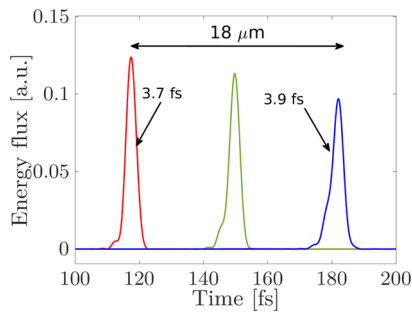
Figure 6. SPP energy flux measured at different propagation distances of the same simulation. As the SPP propagates along the surface, the duration increases due to the dispersion. The parameters of the simulations were the same as in Figure 5.

appears to be related to the pulse impinging in different points of the grating because of the WFR. Different "portions" of the pulse propagate in different directions, and the focus of the pulse is not exactly on the target surface, thus the incidence point (determined by the position of the maximum of the energy flux on the grating surface) is not fixed but moves in time. Depending on the sign of the rotation velocity, the incidence point can move either in the direction of propagation of the SPP or in the opposite direction. In the first case, the laser pulse "follows" the SPP and can sustain its growth, which produces the observed increase of the peak intensity with respect to the SPP excited without WFR. In order to give a further illustration of the effect of the sign of the rotation velocity, in the Supporting Information we show simulations for the "resonant" case at normal laser incidence $\theta = 0°$, corresponding to $d = \lambda$. In the case of a pulse without WFR, in this configuration two counter-propagating SPPs of same amplitude and duration are excited. When adding WFR, only the SPP that propagates in the same direction of the incidence point is generated with high efficiency.

Dispersion effects are weak for SPPs in the typical condition $\omega_p^2 \gg \omega^2$; for our parameters, the phase velocity $v_p = \omega/k = 0.987c$ is only slightly different from the group velocity $v_g = d\omega/dk = 0.96c$. However, in principle also weak dispersion may cause some pulse lengthening with the propagation distance because of the large spectral bandwidth of a few-cycle SPP. We evaluated this effect by a simulation with very high resolution (at the limit of the available computational resources) in order to minimize numerical dispersion effects. Figure 6 shows the profiles of the energy density measured at different positions in the flat region of the target. The SPP duration increases from 3.7 fs to 3.9 fs over a distance of 18 μm, which is not severe enough to prevent applications. The temporal profile of the

SPP field (not shown) also exhibits a slight chirp of the pulse, due to the lower frequencies traveling faster than higher ones.

A simulation with parameters similar to those used in Figure 6 was also performed artificially setting the damping coefficient γ in eq 5 to zero in order to check the effect of dissipative losses. No noticeable differences were observed, which is consistent with the analytical estimate of the SPP absorption length (from the dispersion relation and eq 5) as $\simeq 300$ μm.

In order to test the robustness of the proposed technique and to check the sensitivity of the ultrashort SPP to laser and grating characteristics, a parametric study has been performed measuring the duration of the SPP as a function of the rotation velocity ξ for different values of the laser pulse waist and duration and of the grating pitches, i.e., of the resonant angle θ_R. In these parametric simulations, all parameters are identical but one, in order to study independently their effect on the duration of the SPPs.

Results are summarized in Figure 7. For small values of ξ, the SPP duration increases with the waist size w_0 (Figure 7(a)). This is due to a geometrical effect, since the time needed to propagate across the lit zone, over which the SPP is excited, is not negligible with respect to the laser pulse duration, so that in the absence of WFR the SPP is always longer than the driving pulse. However, for the "optimal value" $\xi = 0.6$ the shortest SPP duration is almost independent of w_0. This might be explained by the WFR velocity being large enough that (roughly speaking) the edges of the laser pulse are out of resonance. This occurs when the effective angle of incidence becomes nonresonant within a laser period, which is consistent with the shortest pulse duration becoming really close to the single-cycle limit.

Reducing the laser pulse duration down to 9.8 fs has the opposite effect on the generated SPP (Figure 7(b)). This is due to the pulse bandwidth becoming larger than the SPP resonance curve, which causes pulse lengthening due to bandwidth loss (as was also observed for a 5 fs input pulse by Dombi et al.[11]). Some dependence on the resonant angle θ_R is apparent (Figure 7(c)). The case $\theta_R = -25°$ appears to be the most suitable for experimental realization since the shortest SPP duration is obtained for not so "extreme" values of ξ.

Finally, the energy flux of the SPP has been measured as a function of the incidence angle θ, to characterize the width in θ of the SPP resonance. Results are shown in Figure 8. The resonance is tighter for a pulse with waist $w_0 = 6\lambda$ ($\Delta\theta_R \simeq 4.7°$) with respect to a pulse with shorter waist $w_0 = 2\lambda$ ($\Delta\theta_R \simeq 10.9°$). This is due to the spread in the wavevector spectrum for a focused pulse, which is on the order of λ/w_0. The pulse bandwidth also contributes to the resonance width because of the relation between θ_R and λ. As also shown in Figure 8, the reference pulse of $\sim$29.5 fs duration and bandwidth of $\sim$23
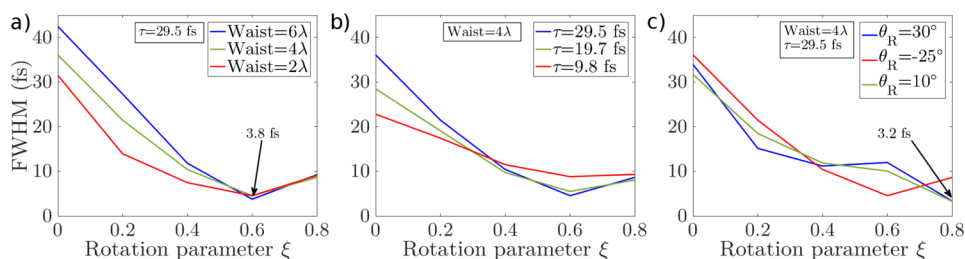
Figure 7. Duration of the SPP at fwhm as a function of the WFR parameter ξ and for different values of the (a) laser pulse waist, (b) laser pulse duration, and (c) grating resonant angle.
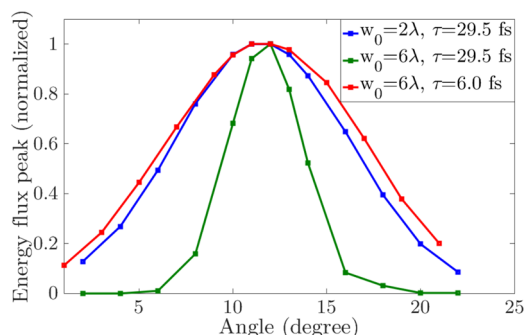
Figure 8. SPP's energy flux peak as a function of the incidence angle for a pulse with waist 2λ and 6λ with a duration of 29.5 fs and for a pulse with waist 6λ and a duration of 6.0 fs. The simulations were performed with a grating having a pitch $d = 0.98$ μm, corresponding to a resonance angle of $\sim 10°$.

THz lead to a tighter resonance than using a pulse of 6.0 fs duration and ~ 105 THz bandwidth, for which $\Delta\theta_R \simeq 12.5°$.

CONCLUSIONS

A proposal for the generation of few-cycle surface plasmon polaritons by laser pulses with wavefront rotation has been investigated via simulations with realistic parameters. Results show that the duration of an SPP can be controlled with the rotation velocity and a "near-single-cycle" SPP of <4 fs duration, corresponding to <1.5 optical cycles of the 800 nm driving laser, can be generated with high amplitude (~ 2.7 times the laser field) and coupling efficiency (>5%). The SPP is so short that carrier-envelope phase effects become important. Moreover the duration is conserved over propagation distances long enough to be suitable for applications.

The experimental realization appears to be straightforward, as it could exploit already tested schemes for WFR[27] based on routinely available laser pulses with ~ 10 cycle duration and standard optical elements. Thus, the experimental setup appears to be simpler and cheaper than those using a few-cycle laser driver, while generating SPPs of even shorter duration. The latter may be characterized by, for example, attosecond photoscopy.[35] The proposed technique may thus be beneficial for several plasmonic applications in the ultrafast and strong field regimes.

METHODS

The simulation campaign was performed with a finite difference time domain code, MEEP.[36] The expression for the WFR laser pulse in the focus was

$$E_{WFR} = E_G(r, z, t)\, \exp[i\omega_L t + itr\xi] \tag{6}$$

where $\xi = 4\frac{w_i \eta}{w_0 \tau_f \tau_i}$ is the rotation parameter. $E_G(r, z, t)$ is the expression that describes the spatial profile of a 2D Gaussian pulse:[37]

$$E_G(r, z, t) = \left(\frac{2w_0^2}{\pi w(z)^2}\right)^{1/4} \exp\left[-\frac{r^2}{w(z)^2} - \frac{t^2}{\tau^2}\right]$$

$$\exp\left[-ikz - ik\frac{r^2}{2R(z)} + i\psi(z)\right] \tag{7}$$

where z and r represent respectively the longitudinal and transverse coordinates, w_0 and τ are the pulse waist and duration, and z_R is the Rayleigh length. $\psi(z)$, $R(z)$, and $w(z)$ are the Gouy phase, the radius of curvature of the wavefronts, and the diameter of the pulse:[37]

$$R(z) = z\left[1 + \left(\frac{z_R}{z}\right)^2\right] \tag{8}$$

$$w(z) = w_0 \sqrt{1 + \left(\frac{z_R}{z}\right)^2} \tag{9}$$

$$\phi(z) = \arctan\left(\frac{z}{z_R}\right) \tag{10}$$

The rotation velocity was controlled varying the rotation parameter ξ. The wavefronts rotate in time with a rotation velocity v_r determined by $v_r(\xi) \simeq 37.7\xi$ mrad/fs, so that the maximum value estimated by Quéré et al.[27] corresponds to $\xi \simeq 0.8$ in our simulations. The box size was 40×30 μm with a resolution of 10 nm.

ASSOCIATED CONTENT

Ⓢ Supporting Information

The Supporting Information is available free of charge on the ACS Publications website at DOI: 10.1021/acsphotonics.7b01347.

> Description of the effect of the rotation direction; dependency of the shortening effect on the rotation direction shown by means of graphics and videos (ZIP)

AUTHOR INFORMATION

Corresponding Authors
*E-mail: f.pisani3@studenti.unipi.it.
*E-mail: luca.fedeli@polimi.it.
*E-mail: andrea.macchi@ino.cnr.it.

ORCID Ⓘ
F. Pisani: 0000-0001-6893-4465
A. Macchi: 0000-0002-1835-2544

Notes
The authors declare no competing financial interest.

REFERENCES

(1) Jain, P. K.; Huang, X.; El-Sayed, I. H.; El-Sayed, M. A. Noble metals on the nanoscale: optical and photothermal properties and some applications in imaging, sensing, biology, and medicine. *Acc. Chem. Res.* **2008**, *41*, 1578−1586.

(2) Berweger, S.; Atkin, J. M.; Olmon, R. L.; Raschke, M. B. Adiabatic tip-plasmon focusing for nano-Raman spectroscopy. *J. Phys. Chem. Lett.* **2010**, *1*, 3427−3432.

(3) McCamant, D. W.; Kukura, P.; Mathies, R. A. Femtosecond time-resolved stimulated Raman spectroscopy: application to the ultrafast internal conversion in β-carotene. *J. Phys. Chem. A* **2003**, *107*, 8208−8214.

(4) Kumar, G. P. Plasmonic nano-architectures for surface enhanced Raman scattering: a review. *J. Nanophotonics* **2012**, *6*, 064503−1.

(5) Keller, E. L.; Brandt, N. C.; Cassabaum, A. A.; Frontiera, R. R. Ultrafast surface-enhanced Raman spectroscopy. *Analyst (Cambridge, U. K.)* **2015**, *140*, 4922−4931.

(6) MacDonald, K. F.; Sámson, Z. L.; Stockman, M. I.; Zheludev, N. I. Ultrafast active plasmonics. *Nat. Photonics* **2009**, *3*, 55−58.

(7) MacDonald, K. F.; Zheludev, N. I. Active plasmonics: current status. *Laser Photonics Rev.* **2010**, *4*, 562−567.

(8) Gramotnev, D. K.; Bozhevolnyi, S. I. Plasmonics beyond the diffraction limit. *Nat. Photonics* **2010**, *4*, 83−91.

(9) Wei, H.; Xu, H. Nanowire-based plasmonic waveguides and devices for integrated nanophotonic circuits. *Nanophotonics* **2012**, *1*, 155−169.

(10) Rewitz, C.; Keitzl, T.; Tuchscherer, P.; Huang, J.-S.; Geisler, P.; Razinskas, G.; Hecht, B.; Brixner, T. Ultrafast plasmon propagation in nanowires characterized by far-field spectral interferometry. *Nano Lett.* **2012**, *12*, 45−49.

(11) Dombi, P.; Irvine, S. E.; Rácz, P.; Lenner, M.; Kroó, N.; Farkas, G.; Mitrofanov, A.; Baltuška, A.; Fuji, T.; Krausz, F.; Elezzabi, A. Y. Observation of few-cycle, strong-field phenomena in surface plasmon fields. *Opt. Express* **2010**, *18*, 24206−24212.

(12) Ceccotti, T.; et al. Evidence of Resonant Surface-Wave Excitation in the Relativistic Regime through Measurements of Proton Acceleration from Grating Targets. *Phys. Rev. Lett.* **2013**, *111*, 185001.

(13) Fedeli, L.; Sgattoni, A.; Cantono, G.; Garzella, D.; Réau, F.; Prencipe, I.; Passoni, M.; Raynaud, M.; Květoň, M.; Proska, J.; Macchi, A.; Ceccotti, T. Electron Acceleration by Relativistic Surface Plasmons in Laser-Grating Interaction. *Phys. Rev. Lett.* **2016**, *116*, 015001.

(14) Fedeli, L.; Sgattoni, A.; Cantono, G.; Macchi, A. Relativistic surface plasmon enhanced harmonic generation from gratings. *Appl. Phys. Lett.* **2017**, *110*, 051103.

(15) Paulus, G. G.; Lindner, F.; Walther, H.; Baltuška, A.; Goulielmakis, E.; Lezius, M.; Krausz, F. Measurement of the phase of few-cycle laser pulses. *Phys. Rev. Lett.* **2003**, *91*, 253004.

(16) Rácz, P.; Irvine, S.; Lenner, M.; Mitrofanov, A.; Baltuška, A.; Elezzabi, A.; Dombi, P. Strong-field plasmonic electron acceleration with few-cycle, phase-stabilized laser pulses. *Appl. Phys. Lett.* **2011**, *98*, 111116.

(17) Krüger, M.; Schenk, M.; Hommelhoff, P. Attosecond control of electrons emitted from a nanoscale metal tip. *Nature* **2011**, *475*, 78−81.

(18) Piglosiewicz, B.; Schmidt, S.; Park, D. J.; Vogelsang, J.; Groß, P.; Manzoni, C.; Farinello, P.; Cerullo, G.; Lienau, C. Carrier-envelope phase effects on the strong-field photoemission of electrons from metallic nanostructures. *Nat. Photonics* **2014**, *8*, 37−42.

(19) Földi, P.; Márton, I.; Német, N.; Ayadi, V.; Dombi, P. Few-cycle plasmon oscillations controlling photoemission from metal nano-particles. *Appl. Phys. Lett.* **2015**, *106*, 013111.

(20) Li, R.; To, H.; Andonian, G.; Feng, J.; Polyakov, A.; Scoby, C.; Thompson, K.; Wan, W.; Padmore, H.; Musumeci, P. Surface-plasmon resonance-enhanced multiphoton emission of high-brightness electron beams from a nanostructured copper cathode. *Phys. Rev. Lett.* **2013**, *110*, 074801.

(21) Polyakov, A.; Senft, C.; Thompson, K.; Feng, J.; Cabrini, S.; Schuck, P.; Padmore, H.; Peppernick, S. J.; Hess, W. P. Plasmon-enhanced photocathode for high brightness and high repetition rate x-ray sources. *Phys. Rev. Lett.* **2013**, *110*, 076802.

(22) Temnov, V. V.; Klieber, C.; Nelson, K. A.; Thomay, T.; Knittel, V.; Leitenstorfer, A.; Makarov, D.; Albrecht, M.; Bratschitsch, R. Femtosecond nonlinear ultrasonics in gold probed with ultrashort surface plasmons. *Nat. Commun.* **2013**, *4*, 1468.

(23) Scrinzi, A.; Ivanov, M. Y.; Kienberger, R.; Villeneuve, D. M. Attosecond physics. *J. Phys. B: At., Mol. Opt. Phys.* **2006**, *39*, R1.

(24) Ye, F.; Merlo, J. M.; Burns, M. J.; Naughton, M. J. Optical and electrical mappings of surface plasmon cavity modes. *Nanophotonics* **2014**, *3*, 33−49.

(25) Maier, S. A. *Plasmonics: Fundamentals and Applications*; Springer, 2007.

(26) Stockman, M. I. Nanoplasmonics: past, present, and glimpse into future. *Opt. Express* **2011**, *19*, 22029−22106.

(27) Quéré, F.; Vincenti, H.; Borot, A.; Monchocé, S.; Hammond, T. J.; Kim, K. T.; Wheeler, J. A.; Zhang, C.; Ruchon, T.; Auguste, T.; Hergott, J. F.; Villeneuve, D. M.; Corkum, P. B.; Lopez-Martens, R. Applications of ultrafast wavefront rotation in highly nonlinear optics. *J. Phys. B: At., Mol. Opt. Phys.* **2014**, *47*, 124004.

(28) Wheeler, J. A.; Borot, A.; Monchocé, S.; Vincenti, H.; Ricci, A.; Malvache, A.; Lopez-Martens, R.; Quéré, F. Attosecond lighthouses from plasma mirrors. *Nat. Photonics* **2012**, *6*, 829−833.

(29) Vincenti, H.; Quéré, F. Attosecond Lighthouses: How To Use Spatiotemporally Coupled Light Fields To Generate Isolated Atto-second Pulses. *Phys. Rev. Lett.* **2012**, *108*, 113904.

(30) Akturk, S.; Gu, X.; Zeek, E.; Trebino, R. Pulse-front tilt caused by spatial and temporal chirp. *Opt. Express* **2004**, *12*, 4399−4410.

(31) Smith, C. L.; Stenger, N.; Kristensen, A.; Mortensen, N. A.; Bozhevolnyi, S. I. Gap and channeled plasmons in tapered grooves: a review. *Nanoscale* **2015**, *7*, 9355−9386.

(32) Gu, M.; Ouyang, Z.; Jia, B.; Stokes, N.; Chen, X.; Fahim, N.; Li, X.; Ventura, M. J.; Shi, Z. Nanoplasmonics: a frontier of photovoltaic solar cells. *Nanophotonics* **2012**, *1*, 235−248.

(33) Barnes, W. L.; Dereux, A.; Ebbesen, T. W. Surface plasmon subwavelength optics. *Nature* **2003**, *424*, 824−830.

(34) Blaber, M. G.; Arnold, M. D.; Ford, M. J. Search for the ideal plasmonic nanoshell: the effects of surface scattering and alternatives to gold and silver. *J. Phys. Chem. C* **2009**, *113*, 3041−3045.

(35) Lupetti, M.; Hengster, J.; Uphues, T.; Scrinzi, A. Attosecond photoscopy of plasmonic excitations. *Phys. Rev. Lett.* **2014**, *113*, 113903.

(36) Oskooi, A. F.; Roundy, D.; Ibanescu, M.; Bermel, P.; Joannopoulos, J. D.; Johnson, S. G. Meep: A flexible free-software package for electromagnetic simulations by the FDTD method. *Comput. Phys. Commun.* **2009**, *181*, 68710.1016/j.cpc.2009.11.008.

(37) Siegman, A. E. *Lasers*; University Science Books, 1986.